RNA stability is regulated by both RNA polyadenylation and ATP levels, linking RNA and energy metabolisms in Escherichia coli

Charlotte Roux, Marvin Ramos-Hue, Marjorie Audonnet, Marie-Pierre Duviau, Sébastien Nouaille, Agamemnon J. Carpousis, Sandrine Laguerre, Eliane Hajnsdorf, Muriel Cocaign-bousquet, Laurence Girbal

RNA stability is regulated by both RNA polyadenylation and ATP levels, linking RNA and energy metabolisms in *Escherichia coli*

Charlotte Roux[1,2], Marvin Ramos-Hue[1], Marjorie Audonnet[1], Marie-Pierre Duviau[1], Sébastien Nouaille[1], Agamemnon J. Carpousis[1], Sandrine Laguerre[1], Eliane Hajnsdorf[2], Muriel Cocaign-Bousquet[1#], Laurence Girbal[1#]

[1] TBI, Université de Toulouse, CNRS, INRAE, INSA, 31077 Toulouse, France

[2] UMR8261, CNRS, Université de Paris, Institut de Biologie Physico-Chimique, 13 rue Pierre et Marie Curie, 75005 Paris, France

Address correspondence to Laurence Girbal, girbal@insa-toulouse.fr and Muriel Cocaign-Bousquet, cocaign@insa-toulouse.fr.

Eliane Hajnsdorf, Muriel Cocaign-Bousquet and Laurence Girbal contributed equally to this article. Author order was determined on the basis of seniority.

Running title: Interconnections between RNA and energy metabolisms in E. coli

Key words: RNA polyadenylation – PAP I – RNA stability – Energy – ATP – Escherichia coli

Word count for the abstract: 231

Word count for the text: 5443

Abstract

The post-transcriptional process of RNA polyadenylation sits at the crossroads of energy metabolism and RNA metabolism. RNA polyadenylation is catalyzed by poly(A) polymerases which use ATP as a substrate to add adenine to the 3'-end of RNAs, which can alter their stability. In *E. coli*, RNA polyadenylation mediated by the major poly(A) polymerase was previously shown to facilitate degradation of individual RNAs. In this study, we performed the first genome-wide study of RNA stability in the absence of PAP I. Inactivation of the *pcnB* gene coding for PAP I led to the stabilization of more than a thousand of *E. coli* RNAs in the form of full-length functional molecules or non-functional fragments. The absence of PAP I altered the energy metabolism, with an almost 20% reduction in ATP levels. To better understand how RNA and energy metabolisms are interconnected, we investigated the role of ATP levels in regulating RNA stability. When we lowered intracellular ATP levels below 0.5mM, many RNAs were stabilized demonstrating the causal link between ATP levels and RNA stability for the first time in *E. coli*. Above this concentration, changes in ATP levels had no impact on RNA stability. We also demonstrated that some RNAs were stabilized when PAP I was inactivated by low ATP availability. These results clearly demonstrate that PAP I mediates an energy-dependent RNA stabilization which may contribute to cell energy homeostasis under energy-limited conditions.

Importance

Poly(A) polymerases are prime targets for understanding the interactions between RNA polyadenylation, RNA stability and cellular energy. These enzymes catalyze the process of RNA polyadenylation, which involves ATP hydrolysis and addition of poly(A) tails to the 3' end of RNAs. 3'end poly(A) extensions potentially facilitate RNA degradation in bacteria. In

this study we inactivated the *pcnB* gene encoding PAP I, the major poly(A) polymerase in *E. coli*, and investigated the effects on RNA stability and energy levels. Our results show for the first time in *E. coli* a genome-wide RNA stabilization in the absence of PAP I, associated with a decrease in ATP levels. We provide the first evidence in *E. coli* of a link between ATP levels and RNA stabilization and demonstrate that this is mediated in some cases by PAP I. PAP I-mediated RNA stabilization at low ATP levels could be a means of energy conservation under energy-limited conditions.

Introduction

RNA degradation is a ubiquitous process that in most cases begins in *E. coli* with endoribonucleolytic cleavages mainly performed by RNase E, RNase III, RNase G, RNase P, RNase LS or RNase Z. 3′-end exoribonucleases (polynucleotide phosphorylase (PNPase), RNase II, and RNase R) then convert the endonucleolytic cleavage products to oligonucleotides that are further degraded to mononucleotides by oligoribonuclease (see references (1-5) for reviews). In some cases, RNA degradation is initiated by 3′-end exoribonucleases (6, 7). RNA degradation can be facilitated by the addition of 3'-end poly(A) tails by poly(A)polymerase I (PAP I), which provides a binding site for 3’-exoribonucleases (8, 9). So far, the effect of PAP I-mediated polyadenylation on RNA stability has only been studied for individual RNAs. The function of the *pcnB* gene, which codes for PAP I, was first identified in studies of plasmid copy number regulation. Antisense RNA I of ColE1-type plasmids and *copA* sRNA of plasmid R1 are destabilized by PAP I-dependent polyadenylation (10-12). PAP I polyadenylation also affects tRNA maturation and degradation because it competes with 3’-exoribonucleases for access to the 3’-end termini of pre-tRNAs (13-16). Polyadenylation by PAP I influences sRNA stability, as described for GlmY and RyhB,

which are involved in the synthesis of glucosamine-6-phosphate and the expression of the *Fur* regulon, respectively (15, 17, 18). Polyadenylation is also involved in mRNA decay, with a number of transcripts (*rpsO*, *rpsT*, *lpp*, *ompA*, *rmf* and *trxA*) (19-23) and mRNAs involved in hyperosmotic stress (*osmY* and *otsA*) (24) and carbon metabolism (*ptsG* and *malT*) (15) becoming more stable in the absence of PAP I. Some mRNAs, such as *rne* and *pnp*, which code respectively for RNase E and PNPase, are destabilized upon PAP I overexpression (25). Although these examples clearly demonstrate that PAP I is involved in regulating the stability of several RNA species, the full scope of the effect of PAP I-mediated polyadenylation on RNA stability has yet to be determined, since changes in RNA stability in response to variations in PAP I activity have never been measured across an entire genome.

At the physiological level, RNA stability depends on growth conditions: overall, mRNA stability is negatively correlated with growth rates (26) and is reduced in the stationary phase (27). Our hypothesis is that the stabilization of mRNAs under slow or no growth could be an energy saving mechanism. This hypothesis is supported by the fact that simultaneous RNA stabilization and ATP decrease have been observed in carbon-starved cells and in cells exposed to sodium fluoride (28, 29). However, the causal link between low ATP levels and RNA stabilization has yet to be established. To our knowledge, the only existing study clearly linking RNA stability and energy status is Vargas-Blanco et al.'s in *Mycobacterium smegmatis* (30). Understanding the relationship between energy and RNA stability is a major research objective in bacterial physiology. In particular the role of ATP-dependent enzymes involved in RNA degradation remains to be elucidated, notably that of PAP I involved in RNA polyadenylation and ATP consumption and therefore sited at the crossroads of energy and RNA metabolisms in *E. coli*.

This article reports the first genome-scale analysis of the effect of PAP I activity on the stability of *E. coli* RNAs. We used a strain with an inactivated *pcnB* gene encoding PAP I to reduce the level of genome-wide polyadenylation (15). We compared the half-lives of 2627 RNAs in the *pcnB* mutant with those measured in the parent strain grown on glucose. The absence of PAP I had a stabilizing effect on *E. coli* RNAs overall. Because PAP I is an ATP-consuming enzyme, we investigated whether PAP I inactivation was related to changes in intracellular ATP levels and, conversely, whether RNA stabilizing effects could be related to changes in ATP levels. Our results provide the first evidence in *E. coli* of a causal link between ATP levels and RNA stabilization and demonstrate that this is mediated in some cases by PAP I.

Results

PAP I inactivation increases overall RNA stability in *E. coli*

MG1655 and MG1655Δ*pcnB* strains were grown exponentially in M9-glucose. The maximal growth rate was reduced in the absence of PAP I (0.57 ± 0.04 h^{-1} for MG1655Δ*pcnB* versus 0.70 ± 0.02 h^{-1} for MG1655). RNA half-lives were measured across the entire genome after inhibiting transcription with rifampicin by RNA-seq analysis at different time points. Half-lives have been determined with a classical linear model fitted on log concentration of RNA. Reliable half-life values were obtained in both strains for 2627 RNAs. These half-lives were significantly higher on average in the *pcnB* mutant than in the parent strain, with a median value of 2.0 min in MG1655Δ*pcnB* versus 1.3 min in MG1655 (Figure 1**;** Wilcoxon-Mann-Whitney test p-value < 2.2E-6). To account for a potential delay in the onset of exponential decay due to a last round of transcription elongation after rifampicin addition (27) and a possible residual RNA concentration at the end of the decay process (31), we also calculated

RNA half-life by introducing a delay before exponential decay with and without a residual baseline (Figure S1). With a median delay of 30 seconds and a median residual concentration of less than 1.5% of the concentration at T0, the introduction of delay and residual baseline decreased the half-life of only some RNAs for MG1655 and MG1655Δ*pcnB*, while allowing significant correlations between reliable half-lives calculated with and without delay (Figure S1A, $R^2 > 0.8$) and with and without delay plus a residual baseline (Figure S1B, $R^2 > 0.5$). The ratios of the half-lives obtained with delay alone (Figure S1A) and with delay plus residual baseline (Figure S1B) are similar to that obtained without delay or residual RNA concentration (Figure 1), indicating that inactivation of PAP I stabilizes RNAs in *E. coli* irrespective of the half-life calculation method. We then used the half-lives calculated with the classic linear model without the delay and the residual concentration for the rest of the study.

Half-life differences were significantly increased for 1403 individual RNAs in the absence of PAP I, whereas only 4 were destabilized (Figure 2A) confirming the destabilizing role of PAP I at the level of individual RNAs. Analysis of RNA-seq data showed that, depending on the RNA, full-length molecules or fragments were stabilized in the *pcnB* mutant (Figure S3). The accumulation of *zapB* fragments in MG1655Δ*pcnB* was confirmed by Northern blot experiments (Figure S4A). Although we are aware that stabilized fragments can be non-functional, we performed functional analysis of stabilized RNAs. Based on a COG functional enrichment analysis, the stabilized transcripts are involved in essential biological processes, such as DNA replication, recombination and repair (80 RNAs), translation and ribosomal structure and biogenesis (77 RNAs), posttranslational modification, protein turnover and chaperones (49 RNAs), wall, membrane and envelope biogenesis (83 RNAs), and cell cycle and division (18 RNAs), and in coenzyme, amino acid and inorganic ion transport and

metabolism (256 RNAs) (Figure 2B). In addition, the *fli*, *flh* and *flg* regulons involved in flagellum assembly were also more stable in the absence of PAP I (Table S1). Stabilization was likewise observed for several transcripts of the RNA degradation machinery including those encoding RNase E, RhlB, PNPase, RNase R, RNase G, RNase II and RppH, and those coding for RNA binding proteins such as Hfq and Rho (Table S1). Many of the stabilized transcripts are involved in defense mechanisms (22 RNAs) in response to environmental stress, including envelope stress (*rcsD* and *rcsB*), osmolarity stress (*envZ* and *ompR*), as well as limitation in oxygen (*arcA* and *arcB*), phosphate (*phoA* and *phoB*), Mg^{2+} (*phoP*), K^{+} (*kdpD*) and nitrogen (*glnL*, *glnG*, *glnD* and *glnB*) or general stress factors *rpoE* and *rpoH* (Table S1). RNA levels before rifampicin addition indicated that only 164 of the 1403 stabilized transcripts had up-regulated expression (Table S1). Analysis of the functional enrichment of the 164 RNAs pointed out four significantly enriched categories: defense mechanisms against specific stresses (8 RNAs, $p = 1.0E^{-4}$), cell wall, membrane and envelope biogenesis (15 RNAs, $p = 4.4E^{-3}$), coenzyme transport and metabolism (10 RNAs, $p = 5.8E^{-3}$) and general function prediction only (18 RNAs, $p = 8.3E^{-3}$). In contrast, the expression of general stress factors (such as the stabilized mRNAs *rpoE* and *rpoH*) and the seven stabilized transcripts linked to the RNA degradation machinery remained unchanged.

Surprisingly, four transcripts, namely *yabQ*, *elaA*, *rcsA* and *cspE*, were destabilized in the absence of PAP I (Figure 2A, Table S1). The gene *cspE* codes for one of the nine CSPs (cold shock proteins) in *E. coli* and was the only CSP gene destabilized in the absence of PAP I activity. Destabilization of *cspE* was associated with a 56% decrease in its concentration (Table S1).

Inactivation of PAP I leads to a decrease in ATP levels in *E. coli*

Because PAP I is an ATP-dependent enzyme (it consumes one molecule of ATP for each A added to the 3'-end of transcripts), we wondered whether inactivation of PAP I might affect intracellular ATP levels. ATP levels were measured using a bioluminescence assay in exponentially growing MG1655 and MG1655Δ*pcnB* cells in M9-glucose (Figure 3). Intracellular ATP levels were significantly (19%) lower in the absence of PAP I (1.09 mM in MG1655Δ*pcnB* versus 1.34 mM in MG1655, p = 2.2E-3).

E. coli RNAs are stabilized at low ATP levels

Based on the recent observation of RNA stabilization at low energy levels in *M. smegmatis* (30), we wondered whether this might also occur in *E. coli*, in which case the overall stabilization observed in the *pcnB* mutant might also be related to a decrease in energy levels. To address this question, we first studied the link between RNA stability and energy levels in the MG1655 strain by changing the ATP level and measuring how this affected the stability of selected RNAs. We adapted the protocol developed for *M. smegmatis* (30) for *E. coli* growing on succinate as the sole carbon source. Succinate was used instead of glucose to make the respiratory chain the main pathway of ATP synthesis (i.e. to ensure ATP was no longer produced by phosphorylation of the glycolytic substrate) and thus maximize the decrease in intracellular ATP level when the respiratory chain was inactivated using DNP (32-34). Briefly, we co-treated exponentially growing *E. coli* MG1655 cells with rifampicin and DNP, an ATP uncoupler (32). We determined the half-lives by quantitative RT-PCR of twelve RNAs at high (0.7 mM DNP treatment) and very low (2 mM DNP treatment) intracellular ATP levels. The selected RNAs differ in CDS length, concentration, stability, genetic environment, function and protein localization and are therefore representative of the range of RNAs present in *E. coli* (Table 1). Treatment with 0.7 mM DNP did not affect the level of intracellular ATP in MG1655 (around 0.9 mM ATP concentration in the absence of DNP, and

in cells treated with 0.7 mM) while treatment with 2 mM reduced it by 86% to 0.13 mM (Figure 4A). Eight (*focA*, *maeA*, *purL*, *torS*, *atpC*, *flu*, GlmZ and *zapB*) of the 12 selected RNAs were significantly stabilized when the ATP level was reduced; and none were significantly destabilized (Figure 4B). The stabilized RNAs had different concentrations and sizes (Table 1), indicating that these two factors known to influence RNA stability (35, 36) were not involved in this case. We also sequenced the total RNA samples corresponding to 0.7 mM and 2 mM DNP. Based on the RNA-seq data of the eight stabilized RNAs, we found that, depending on the RNA, full-length transcripts or RNA fragments were stabilized at low ATP levels (Figure S6). Northern blot experiments confirmed the absence of *zapB* RNA fragments stabilized at low ATP levels (Figure S4B). Altogether, these results demonstrate that a sharp decrease in ATP levels induces RNA stabilization for most of our selected RNAs. This stabilization was also extended to many other RNAs. We determined genome-wide RNA half-lives from RNA-seq data and found that 1769 RNAs were stabilized between 0.7 mM and 2 mM DNP (Figure S7). The RNA stabilization observed at low ATP levels is likely due to the lower activity of ATP-dependent enzymes, which could act directly on RNA stability as part of the RNA degradation machinery or indirectly via other cellular processes.

Contribution of PAP I to RNA stabilization at low ATP levels

We then investigated whether PAP I might be involved in the RNA stabilization observed at low ATP levels. One explanation for this could be that ATP-consuming enzymes, notably PAP I, are inactivated by the low ATP concentrations. To specifically study the involvement of PAP I independently of any changes in activity of other ATP-dependent enzymes in the RNA degradation machinery, we grew *E. coli* cells with high levels of ATP to saturate all ATP-dependent enzymes and then searched for RNAs that were stabilized in the absence of PAP I. The underlying idea is that RNAs stabilized in the absence of the PAP I enzyme (all

other ATP-dependent enzymes being present and functional at high ATP levels) correspond to RNAs that are also stabilized at low ATP levels when PAP I activity is reduced due to low substrate availability. MG1655 and MG1655Δ*pcnB* cells with the required intracellular ATP levels (around 0.6 mM) were obtained by nitrogen limited growth (Figure 5A). We then compared the half-lives measured by quantitative RT-PCR of the twelve selected RNAs in MG1655 and MG1655Δ*pcnB* at similarly high intracellular ATP levels (Figure 5B). Six RNAs (*deaD*, *mhpC*, *torS*, GlmZ, *aceE* and *argT*) were more stable in MG1655Δ*pcnB* than in MG1655, demonstrating that the stability of these RNAs is dependent on PAP I activity. Among these RNAs, *torS* and GlmZ were also stabilized at low ATP levels in MG1655 (see above). Consequently, we can conclude that these RNAs, which are stabilized when only the PAP I enzyme is absent, were probably also stabilized when MG1655 was exposed to low ATP levels, due to a limitation of PAP I activity by the availability of ATP.

In contrast, six other RNAs (*focA*, *maeA*, *purL*, *atpC*, *flu* and *zapB)* had similar half-lives in MG1655Δ*pcnB* and MG1655 at high intracellular ATP levels (Figure 5B), indicating that they are not regulated by PAP I. However, since these RNAs were stabilized at low ATP levels in MG1655, we wondered whether this could be due to the inactivation of RhlB, another ATP-consuming enzyme in the RNA degradation machinery. To test this hypothesis, the half-lives of *focA*, *maeA*, *purL*, *atpC*, *flu* and *zapB* RNAs were measured by quantitative RT-PCR and compared at high ATP levels (to saturate all ATP-dependent enzymes) in the presence and absence of RhlB (Figure 6). At around 0.7 mM ATP (obtained by adding 0.7 mM of DNP), none of the RNAs were more stable in the $RhlB^-$ strain than in the $RhlB^+$ strain indicating that the stability of these six RNAs does not depend on RhlB activity. Altogether, these results show that the stability of *focA*, *maeA*, *purL*, *atpC*, *flu* and *zapB* RNAs does not vary in the absence of PAP I or RhlB. Their stabilization at low ATP levels in MG1655 must therefore be due to the reduced activity of another ATP-dependent enzyme, part of the RNA

degradation machinery (see Discussion) or involved in other cellular processes affecting RNA stability, such as translation.

Correlation between ATP levels and RNA stability depends on ATP levels

To analyze the correlation between ATP levels and RNA stability, we complemented our data on ATP levels and RNA half-lives in DNP-treated strains grown in M9-succinate, with measurements under new conditions to generate a 3 × 6 matrix of three DNP treatments (no, low concentration and high concentration treatment) and six strains, namely wild-type MG1655 and five strains with mutations in the RNA degradation machinery (absence of PAP I, inactivation or not of RhlB, and overexpression or not of PAP I; Figure 7, Table S3). We observed RNA stabilization when ATP levels were reduced, but only for ATP concentrations below 0.5 mM. Above 0.5 mM, changes in ATP levels where not associated with any significant change in RNA stability.

Discussion

This study is the first genome-wide investigation of the effect of PAP I activity on RNA stability in *E. coli* or any other bacterium. Our results clearly demonstrate that PAP I plays a significant role in regulating RNA stability across the genome as a whole. Absence of PAP I was associated with an overall stabilization of RNAs in *E. coli*, with 1403 RNAs becoming more stable and only 4, less stable. Enzymes of the degradation machinery other than PAP I should not be involved in this overall RNA stabilization because of their constant gene expression. We found that depending on the RNA, full-length molecules or decay fragments were stabilized in absence of PAP I. This confirms that PAP I polyadenylation can affect both decay intermediates and full-length transcripts (15, 37). Full-length transcripts may

accumulate because of a slowdown in the initiation of their degradation triggered by 3'-exoribonucleases. Decay fragments stabilization may occur because of a slower turnover when RNA degradation is initiated by endoribonucleolytic cleavage. Decay fragments can be non-functional and therefore probably have less impact on gene expression than the stabilization of functional full-length transcripts. The effect of the type of stabilized RNA molecules on the regulation of gene expression and therefore on the physiology of *E. coli* cells in the absence of PAP I, could be studied more closely, gene by gene, using proteomic approaches.

Functional analysis of the stabilized transcripts showed that they are involved in essential biological functions (*e.g.* replication, recombination, and DNA repair, translation). These stabilized transcripts included members of several two-component systems, including systems involved in specific environmental stress response but not in the general stress response. We therefore ruled out a global stabilization of RNAs due to the general response to stress. Inactivation of PAP I also stabilized transcripts involved in flagellum assembly. These effects could be related to phenotypic features of the *pcnB* mutant, such as its different sensitivity to stress (15, 24, 38, 39) and decreased motility on soft agar (39). These results highlight the fact that PAP I polyadenylation regulates the stability of transcripts involved in a broad range of biological functions in *E. coli*, with a potentially major impact on cell physiology.

We found that global RNA stabilization in MG1655Δ*pcnB* grown on glucose was associated with almost 20% reductions in growth rate and ATP levels. We can rule out that the overall stabilization of the RNAs is the result of the reduction in growth rate in the *pcnB* mutant. RNA stabilization as a function of growth rate is indeed low when the growth rate remains above 0.4 h^{-1} (26) which is the case for the two strains MG1655 and MG1655Δ*pcnB* with 0.7

h^{-1} and 0.57 h^{-1} respectively. We also identified only a very limited number of RNAs (*glyS, fruB; glyQ, cysK, yqjH, tnaA, ulaE, prfB* and *fabA*) stabilized in MG1655Δ*pcnB* and also stabilized when the growth rate decreased from 0.63 to 0.4 h^{-1} (26). Conversely, RNA stabilization can lead to a reduction in growth by reduced release of ribonucleotides when RNA degradation is affected in the *pcnB* mutant, which could limit the synthesis of deoxyribonucleotides and in turn DNA synthesis and growth (40). The decrease in ATP levels in MG1655Δ*pcnB* is rather surprising since in the absence of PAP I, ATP is no longer consumed by the polyadenylation process and the reduced growth rate may indicate a reduction in growth-related energy demand. Given that several di/triphosphate nucleotide synthesis and consumption pathways co-exist in *E. coli* (KEGG database, eco00230 for purine metabolism and eco00240 for pyrimidine metabolism), further experiments to compare nucleotide pools and intracellular energy fluxes in the presence and absence of PAP I are required to fully understand the interaction between RNA polyadenylation, ATP levels and growth rates.

Data in the literature suggest a potential connection between energy status/growth rate and RNA stability regulation in *E. coli* cells (26-29). Our analyses of a selection of RNAs and of the whole RNA population after DNP treatment provide the first evidence of RNA stabilization induced by a sharp decrease in ATP levels in *E. coli* MG1655, with a clear causal link between low ATP levels and RNA stabilization. This causal link has only previously been established in *M. smegmatis* cells (30). In our measurements of ATP levels and RNA half-lives in MG1655 and strains with mutations in the RNA degradation machinery, the stabilizing effect of low ATP levels was only observed below 0.5 mM. This implies that the RNA stabilization observed in the omics study of MG1655Δ*pcnB* at an ATP concentration

above 1 mM was not due to any ATP-level effect on the activity of the RNA degradation machinery.

The ATP level threshold below which RNA stabilization was observed, 0.5 mM, is very close to the Km range reported for PAP I (0.13 mM) and the RNA helicase DbpA (0.33 mM) (41, 42). RNA stabilization at low ATP levels (for example after 2 mM DNP treatment during growth on succinate) may thus be explained by a decrease in the activity of PAP I and RhlB, two ATP-consuming enzymes involved in RNA degradation, due to low substrate availability. We found several RNAs whose stability is indeed PAP I-dependent, including *torS* and GlmZ RNAs, which are destabilized by PAP I. The stability of GlmZ sRNA was already known to be indirectly regulated by PAP I through the polyadenylation of GlmY sRNA (17). The effect of PAP I on *torS* mRNA does not seem to have been reported before, and it is not clear whether this is a direct or an indirect effect. We also identified six RNAs (*focA*, *maeA*, *purL*, *atpC*, *flu* and *zapB*) whose stabilization at low ATP levels did not depend on PAP I activity. For these RNAs, we also excluded a stabilizing effect of RhlB inactivation at low ATP levels. However, we cannot exclude a possible effect of RhlB inactivation on other RNAs that were not investigated here. Although our results indicate that the stabilization of the six RNAs is not related to an ATP effect via substrate limitation of PAP I and RhlB activity, low ATP levels may affect the activity of other enzymes in the RNA degradation machinery: ATP may directly act on RNases as an effector (as with RNase R, which binds but does not hydrolyze ATP for helicase activity *in vitro* (43)) or indirectly via still unknown mechanisms.

At the physiological level, under energy-limited conditions, RNA stabilization could be a means of saving energy by reducing RNA turnover. RNA turnover involves three energy-demanding steps: RNA synthesis, RNA degradation, and regeneration of nucleoside

triphosphates from the nucleoside mono- or diphosphates released by degradation. Our study provides evidence that PAP I is involved in reducing RNA turnover at low ATP levels, by inactivation-induced stabilization of certain RNAs. This result illustrates how the RNA polyadenylation activity of PAP I links the regulation of RNA stability to energy status in *E. coli*.

Materials and methods

Strains and media

The strains and plasmids used in this study are listed in Table 2. We used *E. coli* MG1655 and its derivative MG1655Δ*pcnB*, carrying an inactivated *pcnB* gene, which encodes PAP I (39). PAP I overexpression was obtained by transforming MG1655Δ*pcnB* with the pBMK11 plasmid, carrying *pcnB* under an IPTG-inducible P_{lac} promotor, or the empty plasmid pBMK14 as a control (25). These strains are referred to respectively as MG1655Δ*pcnB*/pPAP I and MG1655Δ*pcnB*/p. RhlB was inactivated by the point mutation DQAD in the DEAD box. First, DNA fragments with appropriate 3' and 5' extensions, synthesized by PCR using genomic DNA as template, were inserted into the chromosome of NCM3416 by λ Red recombination (44). The coding sequence extending from the DEAD-box to the 3' end of the *rhlB* gene (residues 166-421) was deleted by insertion of a *cat* cassette (from pKD3) into NCM3416 to create strain SAJ102. Second, the *rhlB* deletion was repaired in strain SAJ103 by insertion of a *rhlB(DQAD)-kan* DNA fragment that was synthesized by cross-over PCR. The construct was validated by PCR of genomic DNA and sequencing. The *kan* gene (from pKD4), which lacks a promoter and flanking *frt* sites, is co-transcribed with *rhlB*. The genomic fragment containing the *kan* gene was amplified from SAJ103, and used to transform NCM3416 carrying plasmid pKD46, to obtain strain SCR101, with the *kan* gene right after

374 the *rhlB* gene and an intact DEAD box. $RhlB^+$ and $RhlB^-$ were then constructed in MG1655
375 by P1-mediated transduction from SCR101 and SAJ103, respectively. Transductants were
376 selected with kanamycin and confirmed by PCR and sequencing. DNA primers are listed in
377 Table S2.
378 The strains were grown in M9 minimal medium as previously described (26). M9 medium
379 was supplemented with 16.7 mM glucose (M9-glucose) or 85 mM of succinate (M9-
380 succinate). The medium was supplemented with chloramphenicol (20 µg/mL) and IPTG (1
381 mM) if required. Nitrogen limitation was achieved by 6 h of culture in M9-glucose medium
382 containing a 6-fold reduced NH_4Cl concentration (0.34 g/L).
383
384 **Growth conditions on glucose**
385 After overnight precultures in M9-glucose, cells were washed twice with NaCl 9 g/L and used
386 to inoculate 1.8 L of M9-glucose at OD_{600nm}= 0.1 in a Biostat B+ bioreactor. Temperature was
387 regulated at 37°C and pH at 7, and dissolved oxygen pressure was set to a minimum of 30%.
388 When OD_{600nm} reached 1.2, samples were collected for transcriptomic analysis; this time point
389 was defined as the reference time point (T0) for half-life measurements. Rifampicin (0.5 g/L)
390 was then added to the culture to inhibit transcription initiation, and cells were sampled at
391 different times and frozen in liquid nitrogen. These experiments were repeated three times on
392 independent cultures for each strain.
393
394 **Growth conditions on succinate and treatments with rifampicin and DNP**
395 After overnight growth in M9-glucose, cells were washed with M9-succinate, and used to
396 inoculate Erlenmeyer flasks with M9-succinate supplemented with chloramphenicol and
397 IPTG if required at OD_{600nm}= 0.1. At OD_{600nm}= 0.8, rifampicin (0.5 g/L) was added, and cell
398 samples were taken over time and rapidly frozen in liquid nitrogen. When required, cells were

399 treated with either 0.7, 2 or 3 mM 2,4-dinitrophenol (DNP). Rifampicin and DNP were added
400 simultaneously for MG1655, MG1655Δ*pcnB*, M1655pcnB/p and MG1655Δ*pcnB*/pPAP I.
401 Rifampicin was added 15 min after DNP treatment for $RhlB^+$ and $RhlB^-$ to allow ATP levels
402 to decrease. All experiments were performed in biological duplicates and technical triplicates
403 for all strains.
404
405 **RNA extraction**
406 For experiments on glucose, after thawing and centrifugation, the cells were suspended in
407 Tris-EDTA buffer and lysed mechanically with glass beads in the presence of phenol. Total
408 RNA was extracted with TRI Reagent (Sigma Aldrich) from 12 samples from the three
409 biological replicates as follows: for MG1655, T0, 0.5, 2 and 4 min for the first replicate; T0,
410 1, 2.5 and 5 min for the second replicate; and T0, 1.5, 3 and 7 min for the third replicate; for
411 the *pcnB* mutant, T0, 1, 3 and 7 min for the first replicate; T0, 0.5, 1.5 and 5 min for the
412 second replicate; and T0, 2, 4 and 11 min for the third replicate. DNA contamination was
413 removed with a Turbo DNase treatment (Invitrogen). For experiments on succinate, after
414 mechanical lysis with glass beads, total RNA was extracted using the RNeasy Mini Kit
415 (Qiagen) at times T0, 0.4, 1, 2, 4 and 7 min for the two biological replicates. DNA
416 contamination was removed by DNase I treatment.
417
418 **RNA-seq**
419 For experiments on glucose, total RNA was ribodepleted using the riboPOOLs kit (siTOOLs
420 Biotech). 10 ng ribodepleted RNA was further used to construct a sequencing library using
421 the Ion Total RNA-Seq Kit v2 and the Ion Xpres RNA-Seq Barcode Kit (Thermo Fisher
422 Scientific). The library was constructed according to the manufacturer's protocol. 15 pg/µl of
423 each library was amplified by emulsion PCR on the Ion One Touch 2 instrument. Then, a 100

base pair [bp] single-end library was sequenced on an Ion GeneStudio S5 system with an Ion 540 Chip at the GeT-BioPuces platform (http://get-biopuces.insa-toulouse.fr/). For experiments on succinate, total RNA was ribodepleted using the Ribo-Zero kit (Illumina). A paired-end 150 bp sequencing strategy was performed on Illumina PE150 platform (Novogene). Reads were mapped onto the *Escherichia coli* genome (version NC_000913.3, GenBank) with the tmap routine in Torrent and Bowtie2 for Illumina sequencing. Counting was performed with HTSeq-count for Ion torrent sequencing and featureCounts for Illumina sequencing. The linearity range between number of reads and RNA concentration was established above 10 reads using Ambion™ ERCC RNA spikes. To account for a potential effect of the read cutoff values, we have compared the numbers of RNAs with reliable half-life, stabilized RNAs and destabilized RNAs when using read cut-off values of 10 and 100 (Table S4). Increasing read cutoff value decreased the number of reliable RNA half-lives, but did not substantially alter the proportion of stabilized and destabilized RNAs.

Transcriptome

For the transcriptome analysis on T0 samples, transcripts with fewer than 10 reads in 5 of 6 samples were excluded from the analysis, as were duplicated genes and overlapping genes with at least 50 bp in common. A TMM (Trimmed Mean of M values) normalization was applied to correct for experimental variations (45). Differential RNA concentrations were evaluated using an exact test for a difference in means between two groups of negative binomial random variables (45). The p-values were adjusted for multiple testing using the Benjamini and Hochberg false discovery rate method (46). Differences in RNA concentrations were considered significant at $p < 0.01$.

Genome-wide determination of RNA half-lives

Genome-wide measurements of RNA half-lives were performed using 12 sets of RNA-sequencing data (T0 samples and time points after rifampicin addition). The sequencing data were normalized using the first three invariant genes in each strain (genes with the lowest variance in rank between sequencing datasets, (namely b2621 (*ssrA*), b2911 (*ssrS*) and b3760 (*aspT*) on glucose and b2621 (*ssrA*), b3123 (*rnpB*) and b2092 (*gatC*) on succinate). The linear regression coefficient, *k*, of $\log(\mathrm{RNA}) = \log(a_0) - k * t$, with a_0 the RNA concentration à T0, and the associated coefficients of determination, R^2, were calculated for each RNA species. The values obtained for *k* were only considered reliable if the associated R^2 was >70%. RNA half-lives ($t_{1/2}$) were obtained from *k* using the relationship $t_{1/2}$ = 1n2/*k* and were compared using t-tests. Differences were considered statistically significant if the adjusted p-value was < 0.05. The stabilized and destabilized RNAs in MG1655Δ*pcnB* versus MG1655, and the associated concentrations, are listed in Table S1.

Estimation of RNA half-lives by quantitative PCR

A 5 µg sample of total RNA was then retrotranscribed using the SuperScript II Reverse Transcriptase and RNase H (Invitrogen), and complementary DNA was purified on MicrospinG-25 (Cytiva). Quantitative PCR was performed with the primer pairs listed in Table S2, using IQTM SYBR Green Supermix (Biorad) and fluorescence was read using the LightCycler 480 II (Roche). Each quantification was performed in technical duplicates. Primer specificity was determined on a standard range of genomic *E. coli* MG1655 DNAs, and ranged from 85% and 95%. RNA quality was checked using Bioanalyzer 2100 (Agilent). The linear regression coefficient, *k'*, of C_q (quantification cycle) versus time (6 points) and its associated coefficient of determination, R^2, were calculated for each RNA species, for each DNP treatment condition and for each strain. The values obtained for *k'* were only considered reliable if the associated R^2 was > 50%. RNA half-lives were obtained from *k*' using the

relationship $t_{1/2}= 1/k$'. RNAs with a half-life greater than 12 min, or so stable that the half-life could not be reliably quantified, were classified as very stable. Differences in half-lives were tested for statistical significance using Wilcoxon-Mann-Whitney tests on two biological replicates and two technical replicates.

ATP quantification

ATP levels were determined using the BacTiter-Glo Microbial Cell Viability Assay Kit (Promega). After centrifugation of 0.8 mL of culture, the cell pellet was resuspended in 0.8 mL of DNP-supplemented growth medium. Samples (75 µL) were transferred to a black 96-well plate containing 125 µL of BacTiter Glo reagent, shaken for 10 s and incubated for 5 min at room temperature. Luminescence was measured using a Synergy H1 Microplate reader (BioTek). ATP quantification using the BacTiter-Glo Microbial Cell Viability Assay kit was validated by IC-MS/MS measurements using a protocol described previously (47). Intracellular ATP levels were expressed in mM considering 8×10^{11} cells/L at $OD_{600nm} = 1$ and an intracellular volume of 3 fl per cell (48). Differences in ATP levels were tested for statistical significance using Wilcoxon-Mann-Whitney tests on two biological replicates and three technical replicates.

Functional enrichment

Functional categories enriched in transcript subgroups were determined using the hypergeometric test with the Clusters of Orthologous Groups of proteins (COG) database. Enrichments were considered significant at $p < 0.05$.

Data availability: Raw and processed RNA-seq data were deposited in the Gene Expression Omnibus data repository and are accessible with GEO accession number GSE248472 for glucose experiments, and with GEO accession number GSE272651 for succinate experiments.

Acknowledgements

This research was funded by the French National Research Agency [Grants # ANR-18-CE43-0010 and # ANR-23-CE44-0022].

References

1. Andrade JM, Pobre V, Silva IJ, Domingues S, Arraiano CM. 2009. The Role of 3′–5′ Exoribonucleases in RNA Degradation. Prog Mol Biol Transl Sci 85:187-229.
2. Carpousis AJ, Luisi BF, McDowall KJ. 2009. Endonucleolytic Initiation of mRNA Decay in Escherichia coli. Prog Mol Biol Transl Sci 85:91-135.
3. Bechhofer DH, Deutscher MP. 2019. Bacterial ribonucleases and their roles in RNA metabolism. Crit Rev Biochem Mol Biol 54:242-300.
4. Hui MP, Foley PL, Belasco JG. 2014. Messenger RNA degradation in bacterial cells. Annu Rev Genet 48:537-59.
5. Mohanty BK, Kushner SR. 2016. Regulation of mRNA Decay in Bacteria. Annu Rev Microbiol 70:25-44.
6. Mohanty BK, Kushner SR. 2003. Genomic analysis in Escherichia coli demonstrates differential roles for polynucleotide phosphorylase and RNase II in mRNA abundance and decay. Mol Microbiol 50:645-658.
7. Pobre V, Arraiano CM. 2015. Next generation sequencing analysis reveals that the ribonucleases RNase II, RNase R and PNPase affect bacterial motility and biofilm formation in E. coli. BMC Genomics 16:72.
8. Hajnsdorf E, Kaberdin VR. 2018. RNA polyadenylation and its consequences in prokaryotes. Philos Trans R Soc Lond B Biol Sci 373:20180166.
9. Regnier P, Hajnsdorf E. 2009. Poly(A)-assisted RNA decay and modulators of RNA stability. Prog Mol Biol Transl Sci 85:137-185.
10. Soderbom F, Binnie U, Masters M, Wagner EG. 1997. Regulation of plasmid R1 replication: PcnB and RNase E expedite the decay of the antisense RNA, CopA. Mol Microbiol 26:493-504.
11. Xu F, Cohen SN. 1995. RNA degradation in Escherichia coli regulated by 3' adenylation and 5' phosphorylation. Nature 374:180-3.
12. Xu F, Lin-Chao S, Cohen SN. 1993. The Escherichia coli pcnB gene promotes adenylylation of antisense RNAI of ColE1-type plasmids in vivo and degradation of RNAI decay intermediates. Proc Natl Acad Sci U S A 90:6756-60.
13. Li Z, Pandit S, Deutscher MP. 1998. Polyadenylation of stable RNA precursors in vivo. Proc Natl Acad Sci U S A 95:12158-62.

14. Maes A, Gracia C, Hajnsdorf E, Regnier P. 2012. Search for poly(A) polymerase targets in E. coli reveals its implication in surveillance of Glu tRNA processing and degradation of stable RNAs. Mol Microbiol 83:436-51.
15. Maes A, Gracia C, Innocenti N, Zhang K, Aurell E, Hajnsdorf E. 2017. Landscape of RNA polyadenylation in E. coli. Nucleic Acids Res 45:2746-2756.
16. Mohanty BK, Kushner SR. 2010. Processing of the Escherichia coli leuX tRNA transcript, encoding tRNA(Leu5), requires either the 3'-->5' exoribonuclease polynucleotide phosphorylase or RNase P to remove the Rho-independent transcription terminator. Nucleic Acids Res 38:597-607.
17. Reichenbach B, Maes A, Kalamorz F, Hajnsdorf E, Gorke B. 2008. The small RNA GlmY acts upstream of the sRNA GlmZ in the activation of glmS expression and is subject to regulation by polyadenylation in Escherichia coli. Nucleic Acids Res 36:2570-80.
18. Sinha D, Matz LM, Cameron TA, De Lay NR. 2018. Poly(A) polymerase is required for RyhB sRNA stability and function in Escherichia coli. RNA 24:1496-1511.
19. Aiso T, Yoshida H, Wada A, Ohki R. 2005. Modulation of mRNA stability participates in stationary-phase-specific expression of ribosome modulation factor. J Bacteriol 187:1951-8.
20. Coburn GA, Mackie GA. 1996. Differential sensitivities of portions of the mRNA for ribosomal protein S20 to 3'-exonucleases dependent on oligoadenylation and RNA secondary structure. J Biol Chem 271:15776-81.
21. Hajnsdorf E, Braun F, Haugel-Nielsen J, Regnier P. 1995. Polyadenylylation destabilizes the rpsO mRNA of Escherichia coli. Proc Natl Acad Sci U S A 92:3973-7.
22. Haugel-Nielsen J, Hajnsdorf E, Regnier P. 1996. The rpsO mRNA of Escherichia coli is polyadenylated at multiple sites resulting from endonucleolytic processing and exonucleolytic degradation. EMBO J 15:3144-52.
23. O'Hara EB, Chekanova JA, Ingle CA, Kushner ZR, Peters E, Kushner SR. 1995. Polyadenylylation helps regulate mRNA decay in Escherichia coli. Proc Natl Acad Sci U S A 92:1807-11.
24. Francis N, Behera MR, Natarajan K, Laishram RS. 2023. Tyrosine phosphorylation controlled poly(A) polymerase I activity regulates general stress response in bacteria. Life Sci Alliance 6:e202101148.
25. Mohanty BK, Kushner SR. 1999. Analysis of the function of Escherichia coli poly(A) polymerase I in RNA metabolism. Mol Microbiol 34:1094-108.

574 26. Esquerre T, Laguerre S, Turlan C, Carpousis AJ, Girbal L, Cocaign-Bousquet M. 2014.
575 Dual role of transcription and transcript stability in the regulation of gene expression in
576 Escherichia coli cells cultured on glucose at different growth rates. Nucleic Acids Res
577 42:2460-72.
578 27. Chen H, Shiroguchi K, Ge H, Xie XS. 2015. Genome-wide study of mRNA degradation
579 and transcript elongation in Escherichia coli. Mol Syst Biol 11:781.
580 28. Dressaire C, Picard F, Redon E, Loubiere P, Queinnec I, Girbal L, Cocaign-Bousquet M.
581 2013. Role of mRNA stability during bacterial adaptation. PLoS One 8:e59059.
582 29. Murashko ON, Yeh KH, Yu CA, Kaberdin VR, Lin-Chao S. 2023. Sodium Fluoride
583 Exposure Leads to ATP Depletion and Altered RNA Decay in Escherichia coli under
584 Anaerobic Conditions. Microbiol Spectr doi:10.1128/spectrum.04158-22:e0415822.
585 30. Vargas-Blanco DA, Zhou Y, Zamalloa LG, Antonelli T, Shell SS. 2019. mRNA
586 Degradation Rates Are Coupled to Metabolic Status in Mycobacterium smegmatis. mBio
587 10:e00957-19.
588 31. Moffitt JR, Pandey S, Boettiger AN, Wang S, Zhuang X. 2016. Spatial organization
589 shapes the turnover of a bacterial transcriptome. Elife 5.
590 32. Gage DJ, Neidhardt FC. 1993. Adaptation of Escherichia coli to the uncoupler of
591 oxidative phosphorylation 2,4-dinitrophenol. J Bacteriol 175:7105-8.
592 33. Katayama Y, Kasahara A, Kuraishi H, Amano F. 1990. Regulation of activity of an ATP-
593 dependent protease, Clp, by the amount of a subunit, ClpA, in the growth of Escherichia
594 coli cells. J Biochem 108:37-41.
595 34. van Workum M, van Dooren SJ, Oldenburg N, Molenaar D, Jensen PR, Snoep JL,
596 Westerhoff HV. 1996. DNA supercoiling depends on the phosphorylation potential in
597 Escherichia coli. Mol Microbiol 20:351-60.
598 35. Feng L, Niu DK. 2007. Relationship between mRNA stability and length: an old question
599 with a new twist. Biochem Genet 45:131-7.
600 36. Nouaille S, Mondeil S, Finoux AL, Moulis C, Girbal L, Cocaign-Bousquet M. 2017. The
601 stability of an mRNA is influenced by its concentration: a potential physical mechanism
602 to regulate gene expression. Nucleic Acids Res 45:11711-11724.
603 37. Mohanty BK, Kushner SR. 2006. The majority of Escherichia coli mRNAs undergo post-
604 transcriptional modification in exponentially growing cells. Nucleic Acids Res 34:5695-
605 704.
606 38. Francis N, Laishram RS. 2021. Transgenesis of mammalian PABP reveals mRNA
607 polyadenylation as a general stress response mechanism in bacteria. iScience 24:103119.

608 39. Maes A, Gracia C, Brechemier D, Hamman P, Chatre E, Lemelle L, Bertin PN, Hajnsdorf
609 E. 2013. Role of polyadenylation in regulation of the flagella cascade and motility in
610 Escherichia coli. Biochimie 95:410-8.
611 40. Danchin A. 1997. Comparison between the Escherichia coli and Bacillus subtilis
612 genomes suggests that a major function of polynucleotide phosphorylase is to synthesize
613 CDP. DNA Res 4:9-18.
614 41. Betat H, Rammelt C, Martin G, Morl M. 2004. Exchange of regions between bacterial
615 poly(A) polymerase and the CCA-adding enzyme generates altered specificities. Mol Cell
616 15:389-98.
617 42. Moore AF, Gentry RC, Koculi E. 2017. DbpA is a region-specific RNA helicase.
618 Biopolymers 107:e23001.
619 43. Hossain ST, Malhotra A, Deutscher MP. 2015. The Helicase Activity of Ribonuclease R
620 Is Essential for Efficient Nuclease Activity. J Biol Chem 290:15697-15706.
621 44. Datsenko KA, Wanner BL. 2000. One-step inactivation of chromosomal genes in
622 Escherichia coli K-12 using PCR products. Proc Natl Acad Sci U S A 97:6640-5.
623 45. Robinson MD, Smyth GK. 2008. Small-sample estimation of negative binomial
624 dispersion, with applications to SAGE data. Biostatistics 9:321-32.
625 46. Benjamini Y, Hochberg Y. 1995. Controlling the false discovery rate: a practical and
626 powerful approach to multiple testing. Journal of the Royal Statistical Society Series B
627 57:289-300.
628 47. Morin M, Ropers D, Cinquemani E, Portais JC, Enjalbert B, Cocaign-Bousquet M. 2017.
629 The Csr System Regulates Escherichia coli Fitness by Controlling Glycogen
630 Accumulation and Energy Levels. MBio 8.
631 48. Volkmer B, Heinemann M. 2011. Condition-dependent cell volume and concentration of
632 Escherichia coli to facilitate data conversion for systems biology modeling. PLoS One
633 6:e23126.
634 49. Soupene E, van Heeswijk WC, Plumbridge J, Stewart V, Bertenthal D, Lee H, Prasad G,
635 Paliy O, Charernnoppakul P, Kustu S. 2003. Physiological studies of Escherichia coli
636 strain MG1655: growth defects and apparent cross-regulation of gene expression. J
637 Bacteriol 185:5611-26.

638

Table and Figure Legends

Table 1: List of RNAs selected for half-life measurements by RT-qPCR. COG: clusters of orthologous groups. NA: not available. RNA concentrations and half-lives ($t_{1/2}$) are those measured in strain MG1655 by RNA-seq in the omics study.

Gene name	Gene number	Protein/RNA function	COG	CDS length (bp)	Operon	RNA concentration (AU)	$t_{1/2}$ (min)	Protein cellular localization
deaD	b3162	ATP-dependent RNA helicase DeaD	[J] Translation, ribosomal structure and biogenesis	1890	Yes	87	2.1	cytosol
focA	b0904	formate channel transporter FocA	[P] Inorganic ion transport and metabolism	858	Yes	11	1.7	inner membrane
maeA	b1479	malate dehydrogenase	[C] Energy production and conversion	1698	No	61	2.4	cytosol
mhpC	b0349	2-hydroxy-6-oxononatrienedioate hydrolase	NA	867	Yes	1	3.4	cytosol
purL	b2557	phosphoribosylformylglycinamide synthetase	[F] Nucleotide transport and metabolism	3888	No	195	1.1	cytosol
torS	b0993	sensor histidine kinase TorS	[T] Signal transduction mechanisms	2745	No	2	1.5	inner membrane
atpC	b3731	ATP synthase F_1 complex subunit ε	[C] Energy production and conversion	420	Yes	244	NA	inner membrane
flu	b2000	antigen 43 (Ag43) autotransporter	NA	3120	No	21	NA	outer membrane
glmZ	b4456	small regulatory RNA GlmZ	NA	172	No	77	NA	NA
aceE	b0114	pyruvate dehydrogenase	[C] Energy production and conversion	2664	Yes	494	2.3	cytosol
argT	b2310	lysine/arginine/ornithine ABC transporter periplasmic binding protein	[E] Amino acid transport and metabolism	783	Yes	31	2.6	periplasmic space
zapB	b3928	cell division factor ZapB (Z-ring)	[S] Function unknown	246	No	50	1.7	cytosol

Table 2: List of the strains and plasmids used in this study.

Strain	Genotype	Reference
MG1655	*E. coli* K-12, F-, λ-, *rph-1*	CGSC
MG1655Δ*pcnB*	MG1655, Δ*pcnB::kan*	(39)
NCM3416	*E. coli* K12, F-, λ-, *rph+*, *zib*-207::Tn10	(49)
SAJ102	NCM3416, *rhlBΔ(166-421)::cat*	This work
SAJ103	NCM3416, *rhlB(DQAD)- kan*	This work
SCR101	NCM3416, *rhlB(DEAD)- kan*	This work
$RhlB^+$	MG1655, *rhlB(DEAD)- kan*	This work
$RhlB^-$	MG1655, *rhlB(DQAD)- kan*	This work
Plasmid	**Features**	**Reference**
pBMK11	Carries *pcnB* under the IPTG-inducible *lac* promoter	(25)
pBMK14	Same as pBMK11 but without *pcnB*	(25)
pKD3	Chloramphenicol resistance	(44)
pKD4	Kanamycin resistance	(44)
pKD46	ts origin, ampicillin resistance, λ Red recombinase	(44)

Figure 1: Genome-wide RNA stabilization induced by PAP I inactivation. Boxplots of RNA half-lives in *E. coli* MG1655 and MG1655Δ*pcnB* for 2627 RNAs with reliably determined half-lives in both strains. MG1655 and MG1655Δ*pcnB* cells were exponentially growing in M9-glucose in bioreactors. Data points on boxplots are shown with filled black circles, and outliers with open black circles. Wilcoxon-Mann-Whitney test, *** $p < 0.001$.

Figure 2: Differences in RNA half-lives between MG1655Δ*pcnB* and MG1655 and functional enrichment. (**A**) Volcano plot of the log2 fold change (logFC) of RNA half-lives between MG1655Δ*pcnB* and MG1655. The values above the horizontal black line correspond to significant differences in fold change ($p \leq 0.05$). The 1403 RNAs that were stabilized in the absence of PAP I are shown in red and the 4 RNAs that were destabilized are shown in green. The 1220 RNAs with non-significant differences in stability are shown in grey. Semilogarithmic plots illustrating the degradation profiles of stabilized and destabilized RNAs between MG1655 and MG1655Δ*pcnB* are shown in Figure S2. (**B**) Functional enrichment in the 1403 stabilized RNAs in MG1655Δ*pcnB*. For each Cluster of Orthologous Groups of proteins (COG), the bar represents the percentage of significantly stabilized RNAs relative to the total number of genes in that category. The number of significantly stabilized RNAs and the total number of genes in each category are shown to the right of each bar, with the associated p-value in parentheses.

Figure 3: ATP levels. Intracellular ATP concentrations were measured in exponentially growing cells (OD = 1) of MG1655 and MG1655Δ*pcnB* in M9-glucose in flask cultures. ** $p < 0.01$.

Figure 4: RNA stabilization at low ATP levels induced by treatment with DNP in *E. coli* cells. (A) ATP levels in the absence of DNP, and in cells treated with 0.7 mM and 2 mM DNP. **(B)** RNA half-lives. MG1655 cells were grown in M9-succinate in flask cultures. Succinate was used instead of glucose to make the DNP-sensitive respiratory chain the main pathway for ATP synthesis. RNA half-lives were measured by quantitative RT-PCR in cells at high ATP level (cells treated with 0.7 mM DNP) and low ATP level (cells treated with 2 mM DNP). Representative graphs of the quantification cycle (Cq) versus time illustrating the RNA degradation profiles are shown in Figure S5A. * $p < 0.05$, ** $p < 0.01$.

Figure 5: ATP levels and RNA half-lives in MG1655 and MG1655Δ*pcnB* under nitrogen limitation. (A) ATP levels. **(B)** RNA half-lives were measured by quantitative RT-PCR. Representative graphs of the quantification cycle (Cq) versus time illustrating the RNA degradation profiles are shown in Figure S5B. Half-lives longer than 12 min were classified as highly stable. Cells were grown in M9-glucose limited in NH_4Cl to obtain similar intracellular concentrations of ATP in the two strains and saturate all ATP-dependent enzymes. * $p < 0.05$.

Figure 6: ATP levels and RNA half-lives in the presence or absence of RhlB. (A) ATP levels. **(B)** RNA half-lives were measured by quantitative RT-PCR. Representative graphs of the quantification cycle (Cq) versus time illustrating the RNA degradation profiles are shown in Figure S5C. Cells were grown in M9-succinate in flask cultures treated with 0.7 mM DNP. Succinate was used instead of glucose to make the DNP-sensitive respiratory chain the main pathway for ATP synthesis. Half-lives longer than 12 min were classified as highly stable. * $p < 0.05$.

Figure 7: Correlation between ATP levels and RNA stability. ATP levels and the half-lives of twelve selected RNAs were performed in the presence of no, low (0.7 mM) and high (2-3 mM) concentrations of DNP in M9-succinate for strains MG1655, MG1655Δ*pcnB*, $RhlB^+$, $RhlB^-$, MG1655Δ*pcnB*/p, MG1655Δ*pcnB*/pPAP I (values in Table S3). The half-life of each RNA was measured by quantitative RT-PCR and expressed as a fold change relative to the value in MG1655 grown without DNP. Representative graphs of the quantification cycle (Cq) versus time illustrating the RNA degradation profiles are shown in Figure S5. Data points are colored by condition and the 18 conditions are listed on the figure to specify the strains and DNP treatments used. The median value of all the points in a given condition is indicated by a horizontal black bar. Segmented linear regressions on median values are shown in black and the associated standard error ribbons in grey. The difference in slope (a slope value of -1.9 for ATP levels <0.5 mM *versus* a slope value of 0.5 for ATP levels >0.5 mM) was significant p = 3.2 E-3 using the Student's t-test.

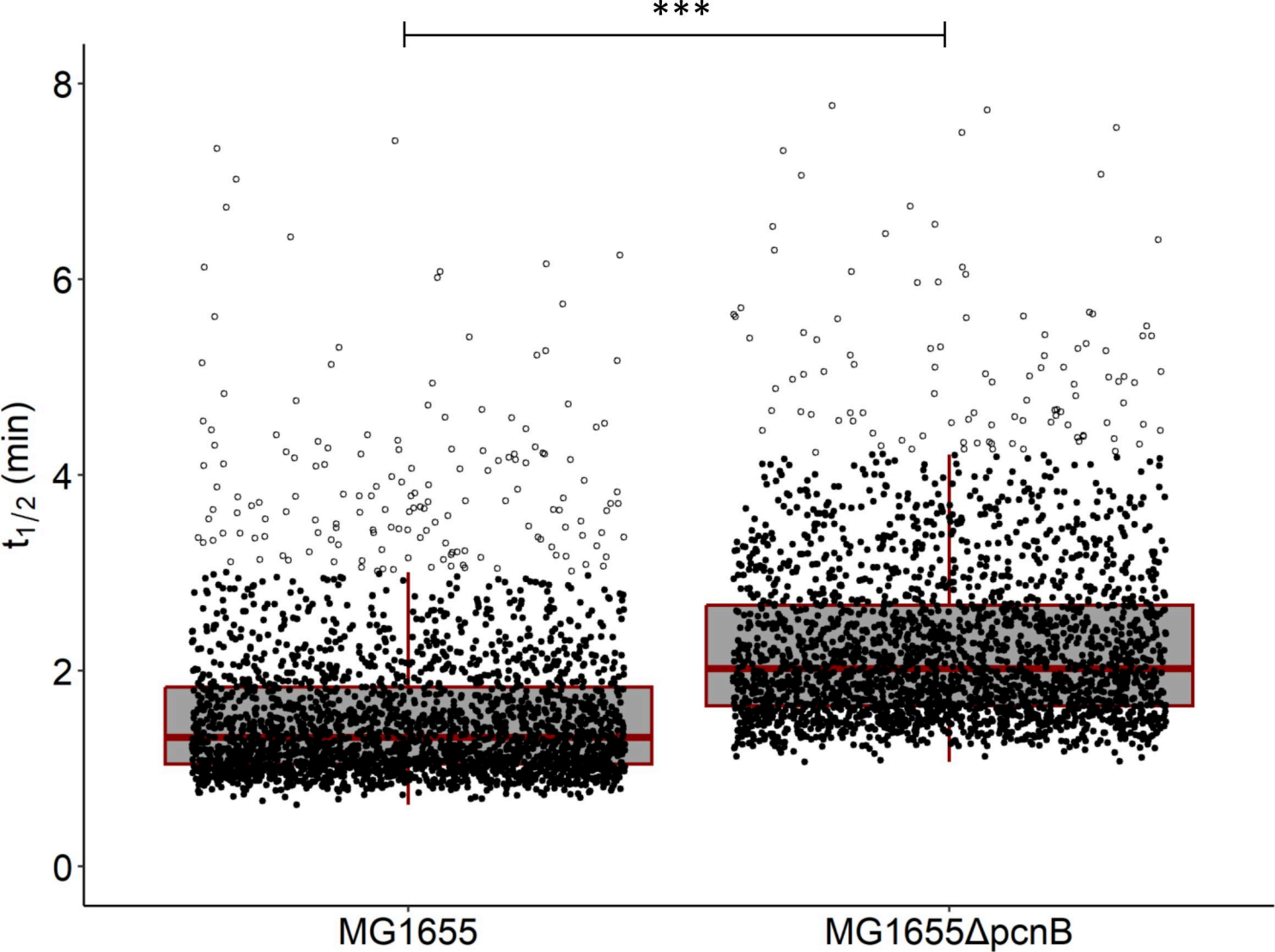
***
8
6
4
2
0
$t_{1/2}$ (min)
MG1655
MG1655ΔpcnB

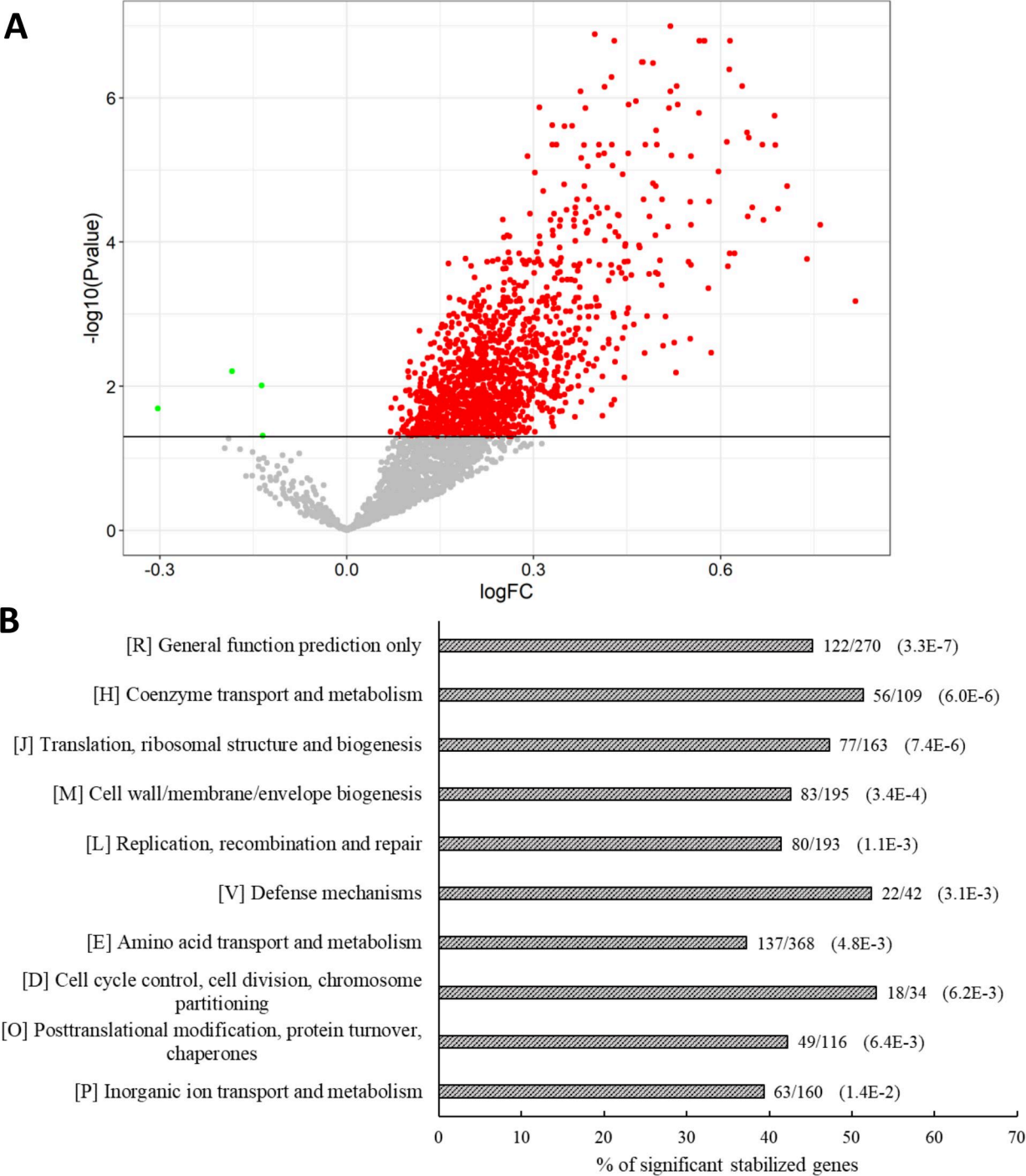
A
-log10(Pvalue)
6
4
2
0
-0.3
0.0
0.3
0.6
logFC
B
[R] General function prediction only
122/270 (3.3E-7)
[H] Coenzyme transport and metabolism
56/109 (6.0E-6)
[J] Translation, ribosomal structure and biogenesis
77/163 (7.4E-6)
[M] Cell wall/membrane/envelope biogenesis
83/195 (3.4E-4)
[L] Replication, recombination and repair
80/193 (1.1E-3)
[V] Defense mechanisms
22/42 (3.1E-3)
[E] Amino acid transport and metabolism
137/368 (4.8E-3)
[D] Cell cycle control, cell division, chromosome partitioning
18/34 (6.2E-3)
[O] Posttranslational modification, protein turnover, chaperones
49/116 (6.4E-3)
[P] Inorganic ion transport and metabolism
63/160 (1.4E-2)
0
10
20
30
40
50
60
70
% of significant stabilized genes

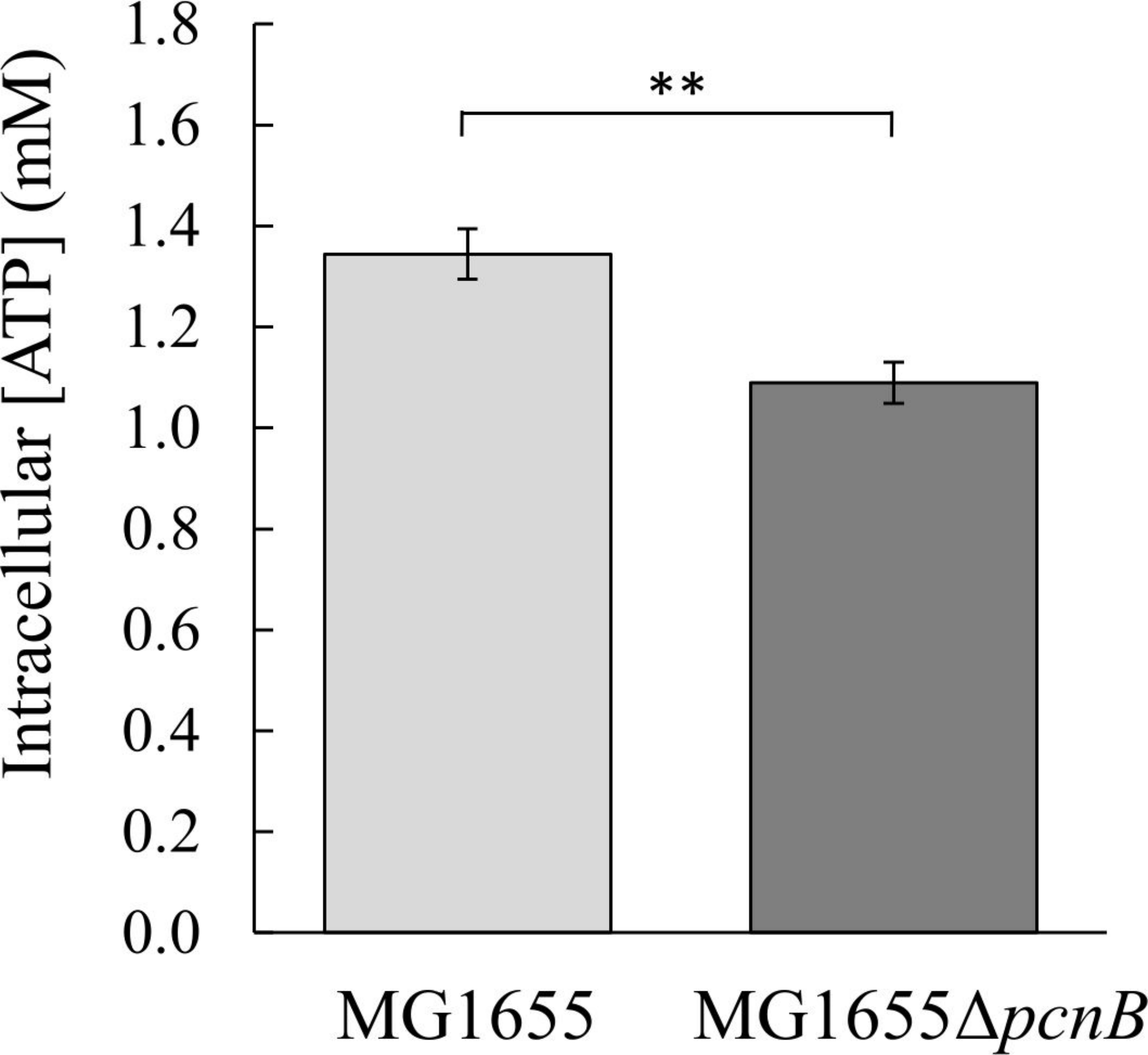
Intracellular [ATP] (mM)
1.8
1.6
1.4
1.2
1.0
0.8
0.6
0.4
0.2
0.0
**
MG1655
MG1655Δpcn B

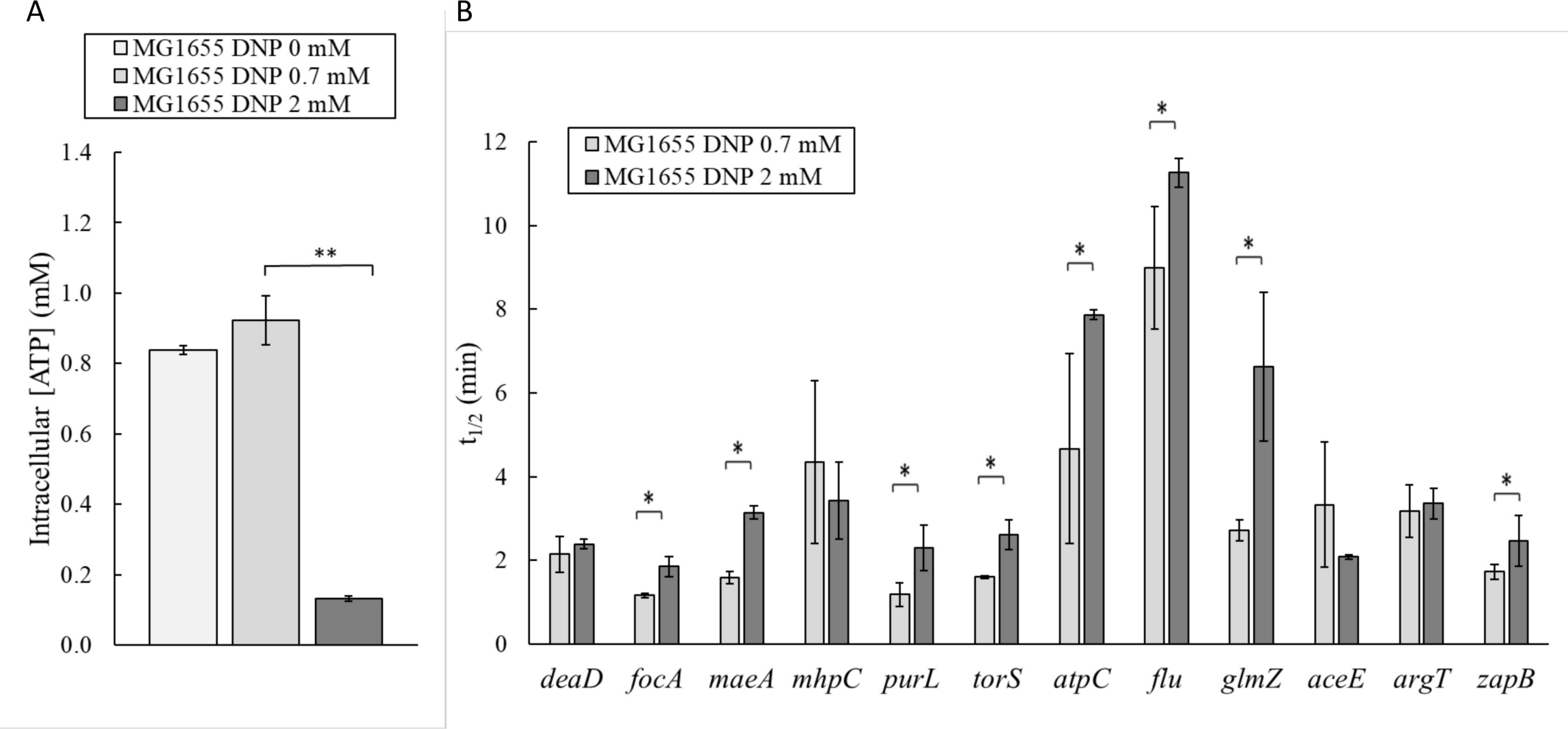
A
MG1655 DNP 0 mM
MG1655 DNP 0.7 mM
MG1655 DNP 2 mM
Intracellular [ATP] (mM)
1.4
1.2
1.0
0.8
0.6
0.4
0.2
0.0
**
B
MG1655 DNP 0.7 mM
MG1655 DNP 2 mM
$t_{1/2}$ (min)
12
10
8
6
4
2
0
*
deaD
focA
maeA
mhpC
purL
torS
atpC
flu
glmZ
aceE
argT
zapB

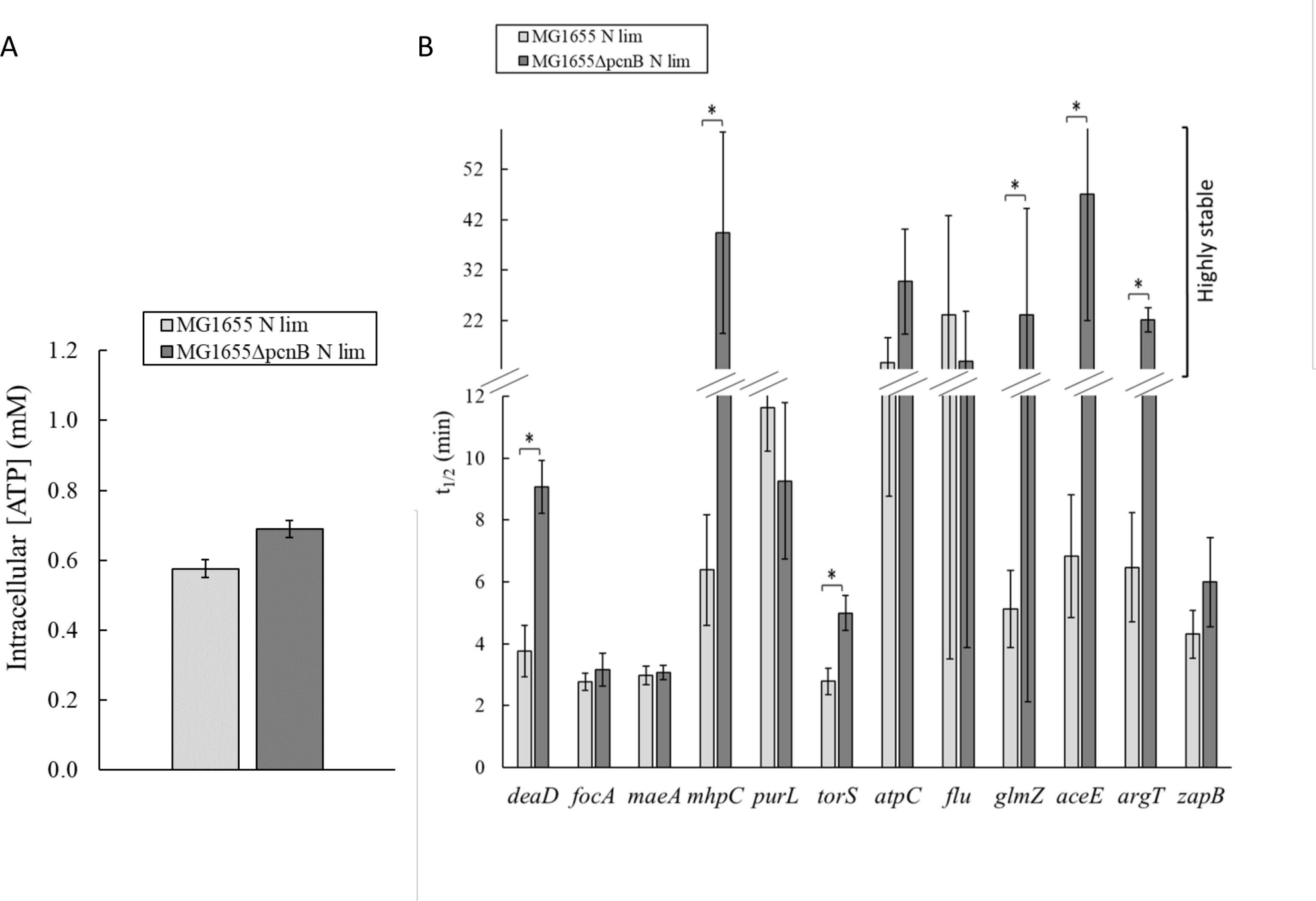
A
MG1655 N lim
MG1655ΔpcnB N lim
Intracellular [ATP] (mM)
1.2
1.0
0.8
0.6
0.4
0.2
0.0
B
MG1655 N lim
MG1655ΔpcnB N lim
$t_{1/2}$ (min)
52
42
32
22
12
10
8
6
4
2
0
Highly stable
*
deaD
focA
maeA
mhpC
purL
torS
atpC
flu
glmZ
aceE
argT
zapB

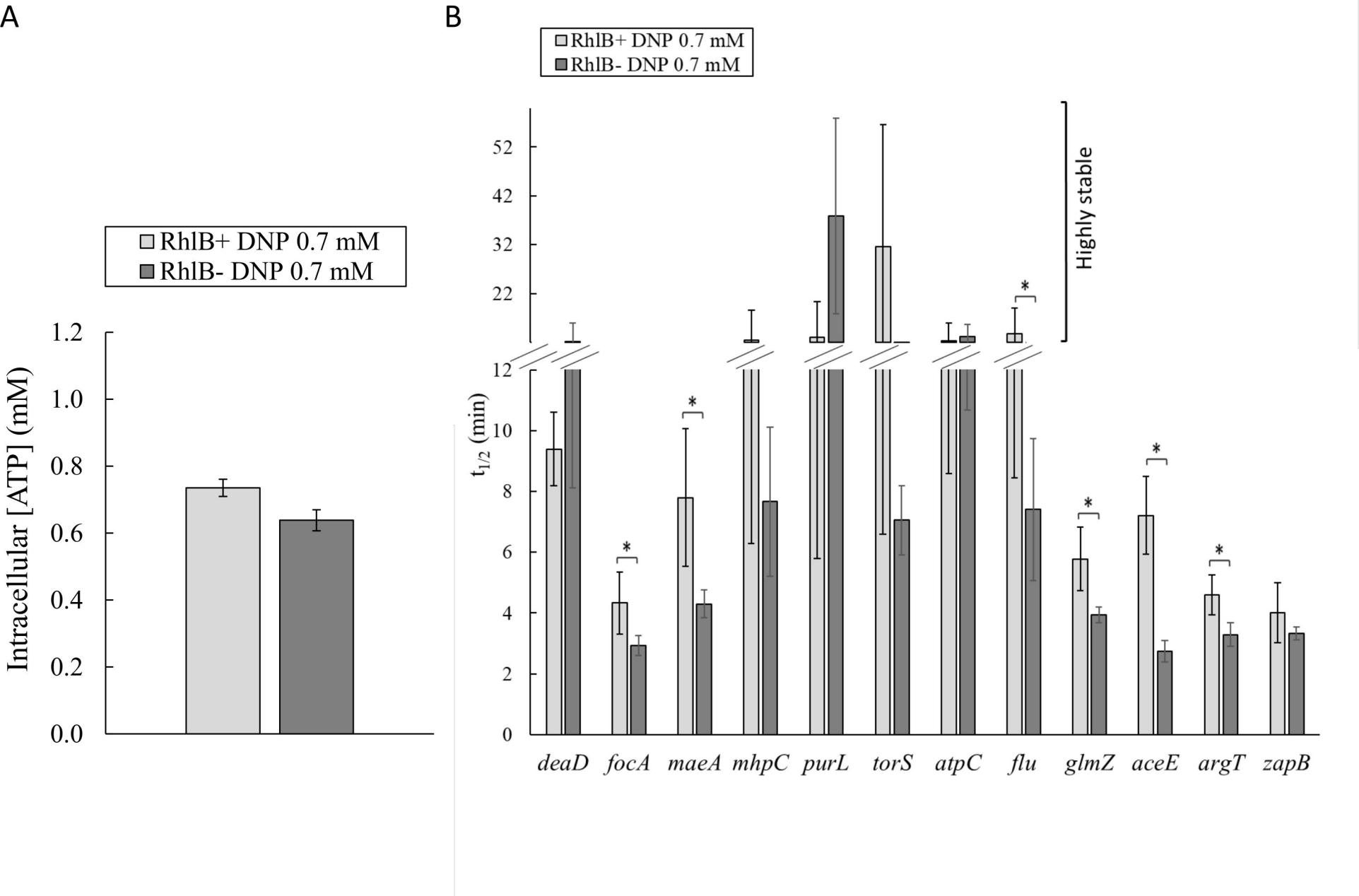
A
RhlB+ DNP 0.7 mM
RhlB- DNP 0.7 mM
Intracellular [ATP] (mM)
1.2
1.0
0.8
0.6
0.4
0.2
0.0
B
RhlB+ DNP 0.7 mM
RhlB- DNP 0.7 mM
Highly stable
$t_{1/2}$ (min)
52
42
32
22
12
10
8
6
4
2
0
*
deaD
focA
maeA
mhpC
purL
torS
atpC
flu
glmZ
aceE
argT
zapB

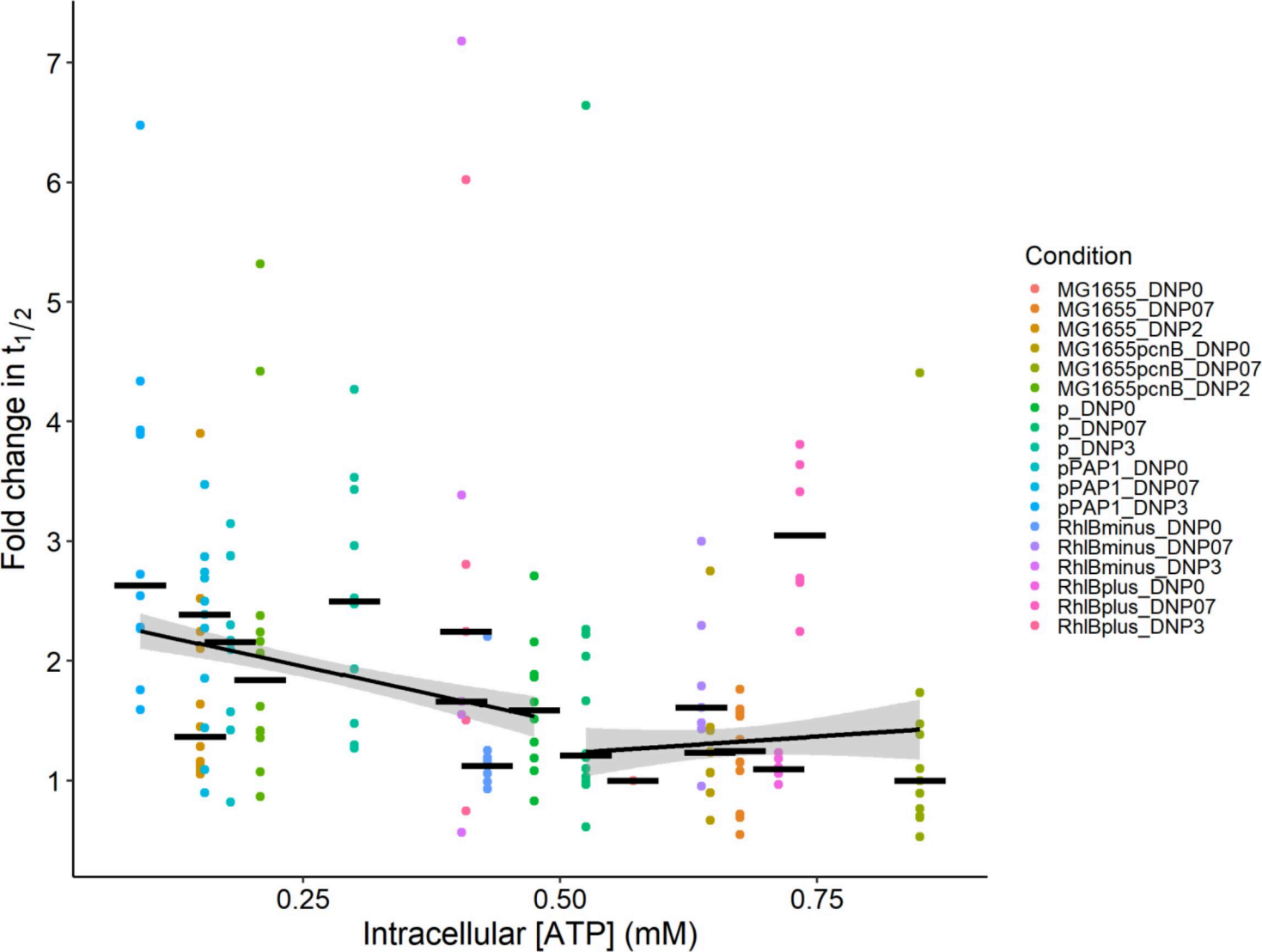
Fold change in $t_{1/2}$
7
6
5
4
3
2
1
0.25
0.50
0.75
Intracellular [ATP] (mM)
Condition
MG1655_DNP0
MG1655_DNP07
MG1655_DNP2
MG1655pcnB_DNP0
MG1655pcnB_DNP07
MG1655pcnB_DNP2
p_DNP0
p_DNP07
p_DNP3
pPAP1_DNP0
pPAP1_DNP07
pPAP1_DNP3
RhlBminus_DNP0
RhlBminus_DNP07
RhlBminus_DNP3
RhlBplus_DNP0
RhlBplus_DNP07
RhlBplus_DNP3